Journal of Sciences, Islamic Republic of Iran 30(1): 41 - 50 (2019) http://jsciences.ut.ac.ir
University of Tehran, ISSN 1016-1104

Fault Strike Detection Using Satellite Gravity Data Decomposition by Discrete Wavelets: A Case Study from Iran

A. Eshaghzadeh[*1], A. Dehghanpour[2], R. Alsadat Kalantari[1]

[1] *Institute of Geophysics, University of Tehran, Islamic Republic of Iran*
[2] *Islamic Azad University, Science and Research Branch, Tehran, Islamic Republic of Iran*

Received: 6 August 2017 / Revised: 3 January 2018 / Accepted: 17 June 2018

Abstract

Estimating the gravity anomaly causative bodies boundary can facilitate the gravity field interpretation. In this paper, 2D discrete wavelet transform (DWT) is employed as a method to delineate the boundary of the gravity anomaly sources. Hence, the GRACE' satellite gravity data is decomposed using DWT. DWT decomposites a single approximation coefficients into four distinct components: the approximation, horizontal, vertical and diagonal. For evaluating the efficiency of wavelets, both the noisy and free-noise synthetic gravity data, have been decomposed at level 1 with six discrete two-dimensional wavelets. In this manuscript, the satellite gravity data of a part of the Makran region (in the south-east of Iran) is decomposed by DWT in order to detect the Saravan Fault trend. The outcome indicates the acceptable performance of the Haar and Biorthogonal mother wavelets in detecting the edges of the real and synthetic gravity anomaly sources. Also, the results demonstrate that the satellite gravity data can be appropriate to study the regional geological structures, particular in revealing the hidden faults where have great importance in earthquake risk analysis.

Keywords: Discrete wavelet transform (DWT); Makran; Saravan Fault; Satellite gravity.

Introduction

In terms of scientific research and engineering operations, gravity exploration has a strong and obvious purpose. The gravity field maps are composed of several wavelengths, since the gravity anomaly sources have different characteristics such as dimensions, density, geometric shapes and structural trends in various depths. both geological discontinuity and structures border imaging are considered as an important step of qualitative and quantitative interpretation of the gravity field maps. Wavelet transform (WT) is widely used in processes such as geophysical data interpretation, signal denoising, separation of potential anomalies and edge detection of subterraneous geological structures. With regard to application, WT can be categorized in two categories: the continuous wavelet transform (CWT) and the discrete wavelet transform (DWT). The wavelet transform is capable of analyzing different frequencies of a signal in various scales so that high frequencies are analyzed in low scales whereas low frequencies are analyzed in high scales. Such said, it enables us to investigate both local and regional geological structures

[*] Corresponding author: Tel: +981152286946; Fax: +981152286946; E-mail: eshaghzadeh.ata@gmail.com

[1].

Fedi and Quata (1998) [2] and *Hornby et al.* (1999) [3] have separated potential anomaly data by means of the wavelet transform. *Leblanc et al.* (1998) [4], *Ridsdill-Smith* and *Dentith* (1999) [5], suggested the use of wavelet filtering techniques in aeromagnetic processing whereas *Trad and Travassos* (2000) [6], recommended wavelets to filter magnetotelluric data. *Holden et al.* (2000) [7] modeled the geometry of geological bodies by multiscale edge analysis and forward modeling methods using wavelet. *Moreau et al.* (1999) [8] used wavelets derived from the Poisson kernel to analyze potential fields and to locate their causative sources. *Deighan and Watts* (1997) [9] applied wavelets for denoising applications to suppress ground roll in seismic records.

Edge detection techniques are used to differentiate some parameters such as the geological discontinuous, direction of the linear geological structures and border between the geological structures and mineral masses. Moreover, numerous techniques have been developed to map and define structural features of gravity data, for instance, the tilt angle (TDR) [10], the Theta map [11], the total horizontal derivative of the tilt angle as an edge detector (THDR) [12], the horizontal tilt angle (TDX) [13], the balanced analytic signal [14] and the normalized horizontal derivative [15]. *Cooper and Cowan* (2009) [16] introduced the terracing method as an operator on potential field data in which sharp boundaries separate the regions of constant field amplitude. *Ferriera et al.* (2013) [17] have shown the efficiency of the tilt angle of the horizontal gradient in the case of qualitative interpretation of magnetic data. *Cooper and Cowan* (2008) [18] suggested using a filter based on the ratio of related normalized standard deviations (NSTD) to make large and small-amplitude edges visible simultaneously. *Li et al.* (2013) [19] indicated the enhanced mathematical morphology filter as edge detector in potential-field data. *Eshaghzadeh* (2015) [20] demonstrated the acceptable performance of the tilt angle of the total horizontal gradient normalized by the analytic signal as an image edge detector of the gravity field. Eshaghzadeh (2016) [21] proposed a new local phase filter namely the tilt angle of the balanced total horizontal derivative for gravity anomalies edge intensification. *Pal and Majumdar* (2015) [22] applied the first vertical derivative, second vertical derivative, analytical signal and tilt angle or derivative for geological appraisal over the Singhbhum-Orissa craton, India using GOCE, EIGEN6-C2 and in situ gravity data. *Satya et al.* (2016) [23] delineated structural features over a part of the Bay of Bengal using total and balanced horizontal derivative techniques.

In this study, 2-D discrete wavelet transform is applied as an edge detection method. The appropriate mother wavelets, which performs best in terms of the synthetic gravity data decomposition, with and without added random noise are determined. Afterwards, to model the Saravan Fault strike, the satellite gravity data of an area in south-east of Iran are decomposed by DWT.

Materials and Methods

Discrete wavelet transform (DWT)

The discrete wavelet transform (DWT) is a linear transformation that operates on a data set, transforming it into a numerically different matrix of the same size and analyzing the properties of a data set as a function of both time (or position) and scale. As a matter of fact, it is a mean by which data are separated into different frequency components, and then studies each component with resolution matched to its scale.

Mallat (1989) [24] introduced an efficient algorithm known as DWT. Based on the theory of multi-scale analysis, the DWT to the gravity data can be performed

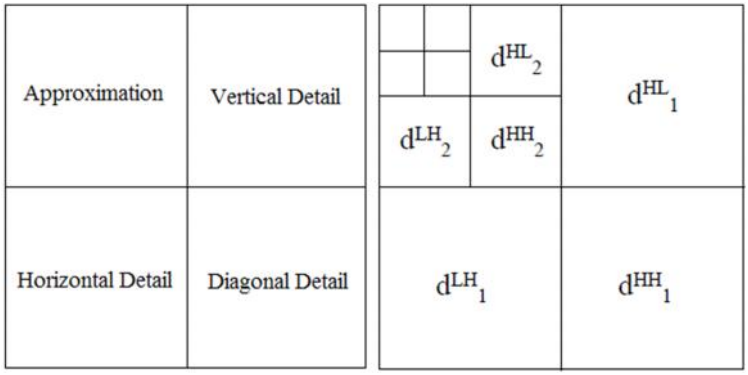

Figure 1. primary steps of the decomposition wavelet transform. The DWT decomposites a single approximate coefficients at level j into four components: the approximation at level j+1, and the details in three orientations (horizontal, vertical, and diagonal).

to decompose the gravity data on different scales (or levels). In this research, orthogonal wavelet transform is used, because it decomposes an input data into a set of independent coefficients, such as approximation (A), vertical (V), diagonal (D) and horizontal (H) details related to each orthogonal basis. Thus, DWT decomposits of the approximate coefficients at the j level in four distinct components in an image: the approximation a^{LL}_{j+1} and details according to three orientations, horizontal d^{LH}_{j+1}, vertical d^{HL}_{j+1} and diagonal d^{HH}_{j+1}, at the level j + 1, where the size of each part is reduced by the factor of two compared to the input image as depicted by Figure 1. The horizontal detail coefficients, vertical detail coefficients and diagonal detail coefficients contain the horizontal, vertical and diagonal components of the input data.

Each wavelet $\psi_{a,b,}$ is defined by the scaling and shifting of the mother wavelet or wavelet function ψ as follows:

$$\Psi_{a,b,}(x) = \frac{1}{\sqrt{a}}\Psi\left(\frac{x-b}{a}\right) \quad (1)$$

Where a and b are scaling (or level or dilation) and shifting (or position or translation) parameters, individually. For certain mother functions, the set of wavelets $\psi_{a,b}$ forms a smooth and orthogonal basis. The 2D wavelet transform is used to describe the wavelets defined in Eq. (1) as basic functions [25]:

$$w_{ab}(x,y) = \frac{1}{\sqrt{a}}\int_{-\infty}^{\infty}\int_{-\infty}^{\infty} g(x,y)\Psi_{ab}(x,y)dxdy \quad (2)$$

Eq. (2) is also called wavelet decomposition of the f(x) using the set of wavelets $\psi_{a,b}$. For that reason, the set of all wavelet coefficients w(a,b) gives the wavelet domain representation of the f(x). This transform is called a discrete wavelet transform (DWT) providing that parameters a, b in Eq. (2) are integer values, otherwise it is called a continuous wavelet transform (CWT).

The scaling function ζ(x) and the corresponding wavelet ψ(x) are defined [26]

$$, (x) = \sum_{k=0}^{N-1} c_k , (2x-k) \quad (3)$$

$$\cdot (x) = \sum_{k=0}^{N-1} (-1)^k c_k , (2x+k-N+1) \quad (4)$$

Where, N is an even number of wavelet coefficients c_k, k=0 to N−1. t_1 and t_2 are the 2-D coordinates and L=low-pass, H=high-pass. Then, the 2-D separable scaling function is [26]

$$, _1(t_1,t_2) = , (t_1), (t_2), \rightarrow LL \quad (5)$$

2-D separable wavelets are,

$$\cdot _2(t_1,t_2) = , (t_1)\cdot (t_2), \rightarrow LH \quad (6)$$

$$\cdot _3(t_1,t_2) = \cdot (t_1), (t_2), \rightarrow HL \quad (7)$$

$$\cdot _4(t_1,t_2) = , (t_1), (t_2), \rightarrow HH \quad (8)$$

A schematic view of 2-D separable wavelets is given in Figure 2. DWT is computed with a cascade of filtering followed by a factor 2 subsampling (Figure 2). In Figure 1, *H* and *L* denotes high and low-pass filters respectively, ↓2 represents subsampling. The DWT is performed firstly for all image rows and then for all columns.

To enhance the anomaly, edge is utilized from the square root of the sum of the squares of the horizontal (H) and vertical (V) components. In the 2D plane, HVC function is given by:

$$HVC = \sqrt{H^2 + V^2} \quad (9)$$

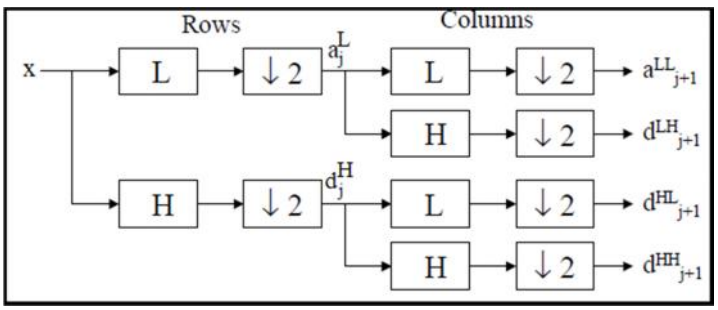

Figure 2. 2D DWT for first level. *H* and *L* denote high and low pass filters respectively, ↓2 denotes subsampling.

In this paper, the first level of wavelet decomposition is used for original data.

Mother wavelets

In wavelet transform, all basic functions called wavelets are derived from scaling and translation of a single function, known as mother wavelet. There are several types of mother wavelets and associated wavelets [27]. In addition, Wavelets have specific properties that make them appropriate for signal processing. As a mathematical tool, information are obtained from various types of data by wavelets. In this study, the application of six discrete wavelet families including Haar, Biorthogonal, Coiflets, Symlets, Discrete Meyer and Daubechies are examined for the decomposition of gravity data set. The selected wavelets characteristics have been presented in Table 1. In fact, the wavelet coefficients are given as the inner product of the function being transformed with each basic function.

DWT of synthetic gravity data set

In this section, the computed gravity field of a model including two prisms at a depth to the top of 2 km (labeled 1) and 4 km (labeled 2) in a 200 km×200 km network is considered. In addition, the density contrast of prisms is assumed to be 1000 kg/m^3. Figure 3 depicts the theoretical total gravity field map due to the two vertical prisms. This part of research aims to evaluate the performance of the wavelet transform technique in edge and corner detection of the gravity anomaly sources that is the prisms here. The images *a* to *k* of Figure 4 represent the DWT using the Bior1.3, Bior1.5, Bior3.1, Bior3.3, Coif1, Db2, Db3, Dmey, Haar, Sym2 and Sym3 wavelets by which a gravity data set at level 1 in four components has been decomposed: the

Table 1. The properties of the discrete wavelets

Wavelet Family	Wavelet	Properties
Haar	Haar	Asymmetric, orthogonal, biorthogonal
Biorthogonal (bior)	Bior1.3	Symmetric, not orthogonal, biorthogonal
	Bior1.5	
	Bior3.1	
	Bior3.3	
Coiflets (coif)	Coif1	Near symmetric, orthogonal, biorthogonal
Daubechies (db)	Db2	asymmetric, orthogonal, biorthogonal
	Db3	
Symlets (sym)	Sym2	Near symmetric, orthogonal, biorthogonal
	Sym3	
Discrete Meyer (dmey)	Dmey	Symmetric, orthogonal, biorthogonal

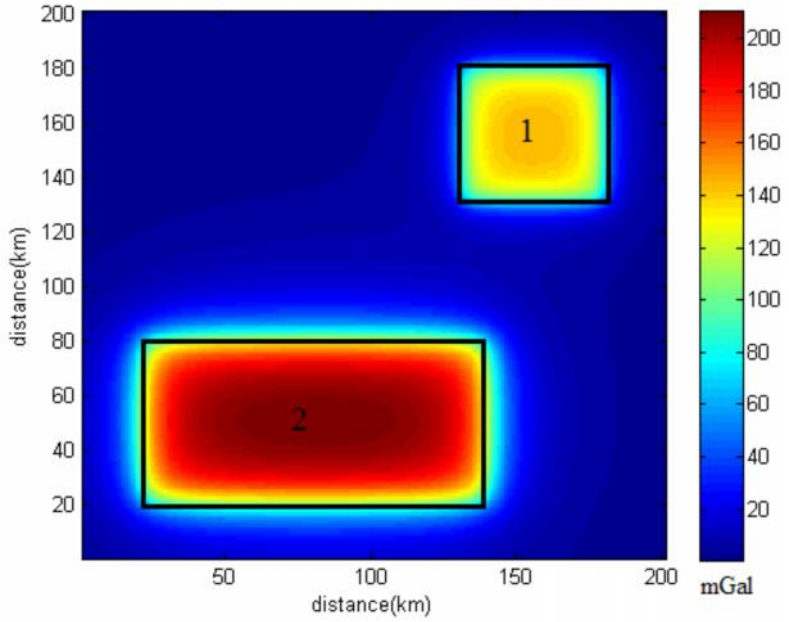

Figure 3. Total gravity field anomaly of vertical prism models of 2 km (prism 1) and 4 km (prism 2) depth

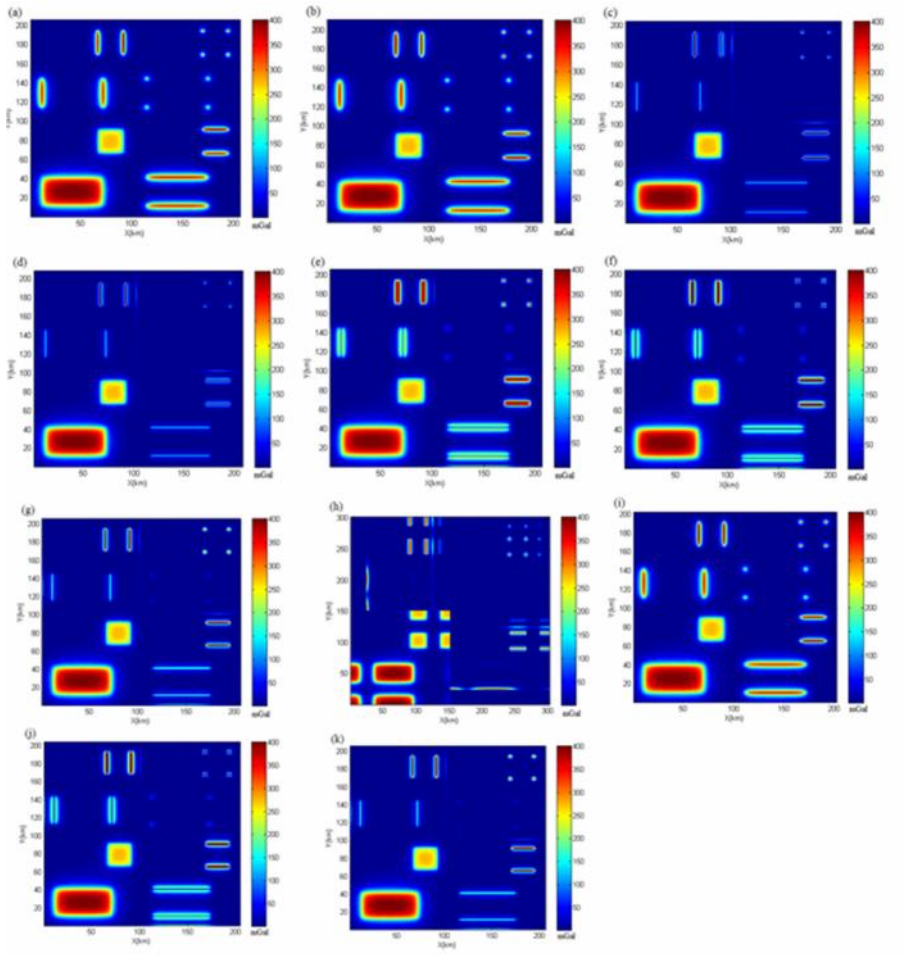

Figure 4. The DWT of the gravity data in figure 3 using the mother wavelets a) Bior1.3 b) Bior1.5 c)Bior3.1 d)Bior3.3 e)Coif1 f)Db2 g)Db3 h)Dmey i)Haar j)Sym2 and k)Sym3, respectively.

approximation coefficients (bottom left) and the details in three orientations: horizontal (bottom right), vertical (top left) and diagonal (top right), respectively. The HVC is computed from the square root of the sum of the squares of the 1st order wavelet detail coefficients produced. Figure 5*a* to *k* show the HVC corresponding to Figure 4*a* to *k*.

Figure 6 illustrates the theoretical gravity anomaly map of that provided in Figure 3 while a Gaussian distribution of 5% random noise has been added to it. The responses of the Haar and Bior1.5 mother wavelets to noise corrupted data appears to be similar. As seen, Figures 7a and 7a indicate the DWT and HVC of the noisy gravity data using the mother wavelets Haar and Bior1.5, respectively. On the other hand, Figures 7b and 8b display the DWT and HVC of the noisy gravity data using the Bior1.3, Bior3.1, Bior3.3, Db2, Db3, Dmey, Sym2 and Sym3 mother wavelets where the outputs are analogous. The results of the DWT and HVC by the coif1 mother wavelet are given through Figures 7c and 8c, respectively.

Field example

The area under investigation is located in south-east of Iran. Actually, this region of Iran is a subduction zone, which is nominated the Makran, where the oceanic crust of the Oman Sea is subducting beneath the Eurasian plate. In this zone, due to presence of several active faults some earthquakes take place each year. Figure 9 exhibits the satellite image of study region in Makran. One of those seismic active faults is Saravan Fault, as seen in Figure 9.

The Saravan Fault with N135˚-145˚ trend is located on the north edge of Quaternary alluviums of the Makran basin. These sediments mostly include wind blow sand deposits and silty outwash deposits. Clearly, present morphology is reflecting the erosion and geological processes particularly in Quaternary age [28]. Figure 10 shows the geological map of Saravan.

This fault with 270 km in length has been extended

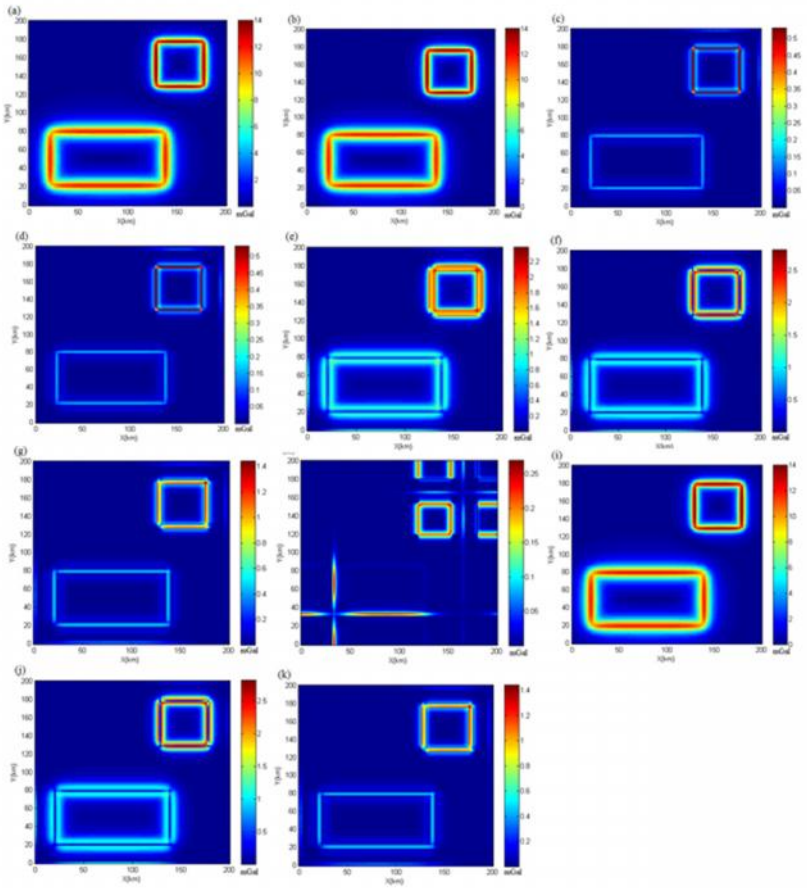

Figure 5. The HVC corresponding to figures 4a to k.

N50W generally and about 50 kilometers of the eastern fault (spacing of Dehak village to Pakistan border) has been also extended along east to west. The rock units of this region are mainly composed of Eocene Flysch. The fault dip angle is approximately at the same direction with flysch layering and its dipping to north-east in 45-60 degree.

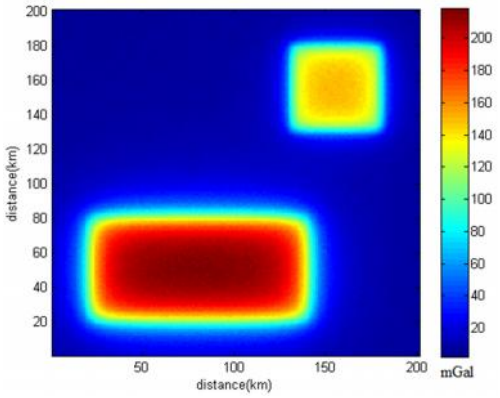

Figure 6. The theoretical gravity field anomaly map with added Gaussian random noise of 5%.

Satellite gravity data decomposition

In this research, gravity data of the GRACE satellite is used. The GRACE data have been extracted from the International Centre for Global Earth Models (ICGEM). The gravity sampling interval of 0.04 degree has been performed inside the restricted area by the black rectangle, as evident in Figure 9. This region is situated between Longitudes 61ºE and 63ºE, Latitudes 27ºN and 29ºN. Figure 11 expresses the satellite Bouguer gravity anomaly map of the area. The Bouguer map shows two major gravity anomalies, where the positive and negative anomalies are placed in the eastern and western part of region, respectively. The residual gravity anomalies were computed removing a polynomial trend from the Bouguer anomalies (Figure 12). The gravity anomalies caused by the geological structures are appeared on the residual gravity field map. As a matter of fact, the strike of the long and active faults on the ground are not a narrow band. Also, of note, is that the contact surface is not a sharp and distinguished surface rather than one determined with the fault zone where the high deformation of material is shown. The hanging

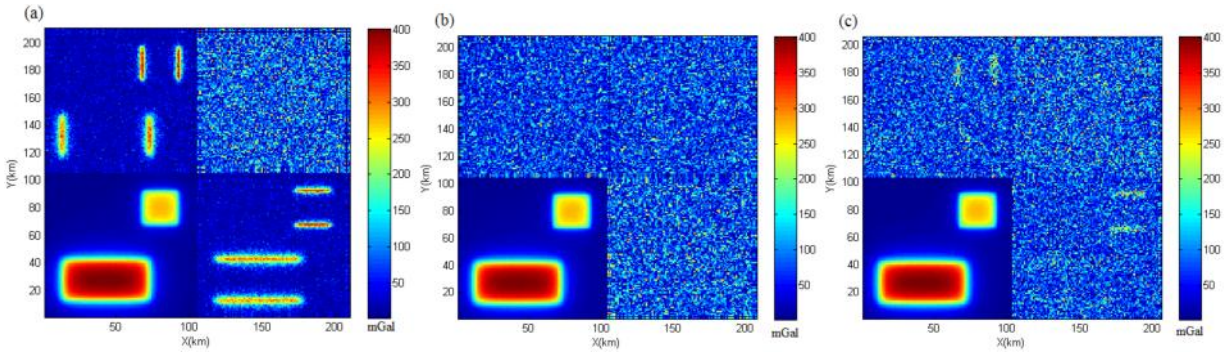

Figure 7. The DWT of the noise corrupted synthetic gravity data using a) Bior1.5 and Haar, b)Bior1.3, Bior3.1, Bior3.3, Db2, Db3, Dmey, Sym2 and Sym3 c)Coif1 mother wavelets.

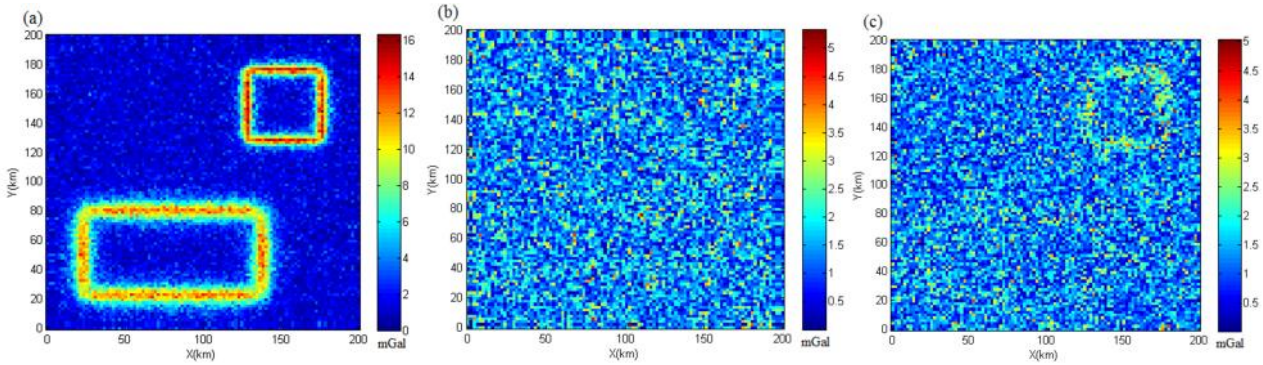

Figure 8. The HVC of the results of the DWT in figure 7 using a) Bior1.5 and Haar, b)Bior1.3, Bior3.1, Bior3.3, Db2, Db3, Dmey, Sym2 and Sym3 c)Coif1 mother wavelets.

wall and foot wall of the reverse faults, such as Saravan Fault on the residual gravity map are specified with the positive and negative anomalies, separately. Therefore, the border of positive and negative anomalies conincides with the strike of dip-slip faults.

The residual gravity data was decomposed using the Haar and Bior 1.5 mother wavelets. Figures 13a and b exhibit the approximation coefficients (A), horizontal (H), vertical (V) and diagonal (D) components at level 1 from the residual gravity data by the Haar and Bior 1.5 mother wavelets, respectively. The HVC of the components of the gravity data DWT by the Haar and Bior 1.5 wavelets are demonstrated in Figures 14a and b, respectively. The location of the Saravan Fault as a linear anomaly causative has been shown on the HVC maps by the red streak. The trend of the HVC maximum values, dashed line, display a good correlation with the length of the Saravan Fault. The HVC has been delineated to linear anomalies in the south-west part of the area under study, as revealed by the black lines in Figure 14. It is worth mentioning that the anomaly where length is longer exhibits the Birg fault.

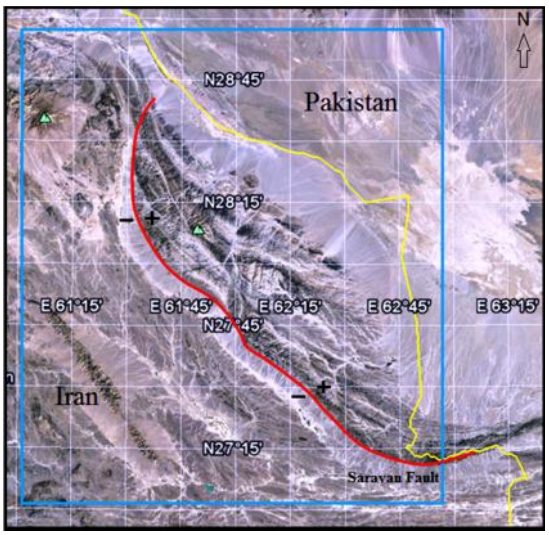

Figure 9. Satellite image of area under study. The red line shows the Saravan Fault strike.

The solutions of the Euler deconvolution always are placed on the edge of the linear geological features. The black points and white lineament on the residual gravity map show the situation of the Euler solutions and the Saravan Fault strike, respectively (Figure 15). The Euler responses have detected the trend of the Saravan Fault approximately, but with unrecognizable contact edge.

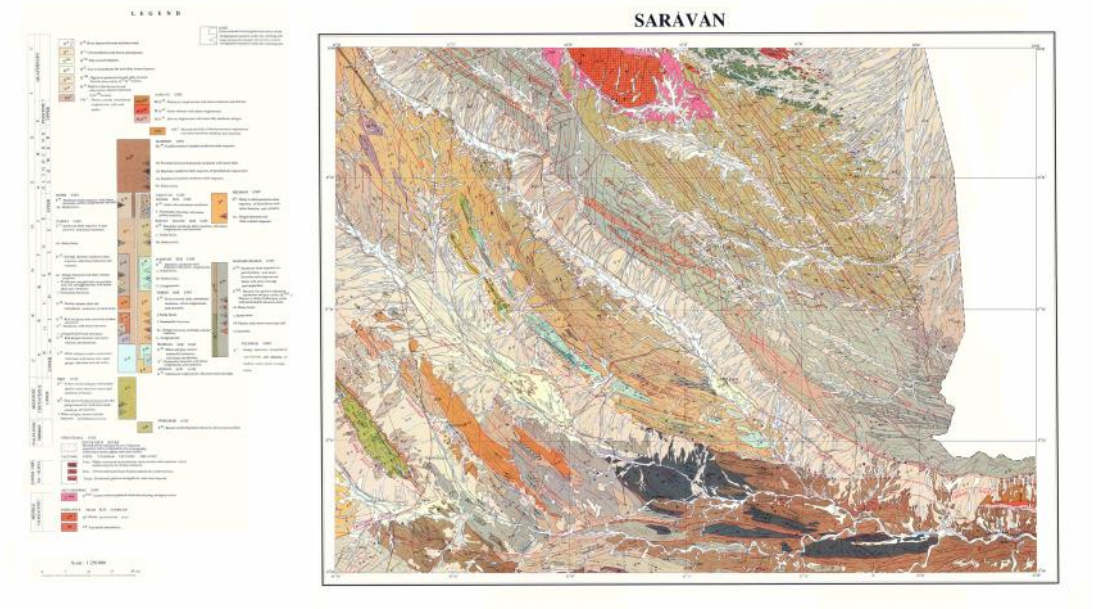

Figure 10. The geological map of Saravan

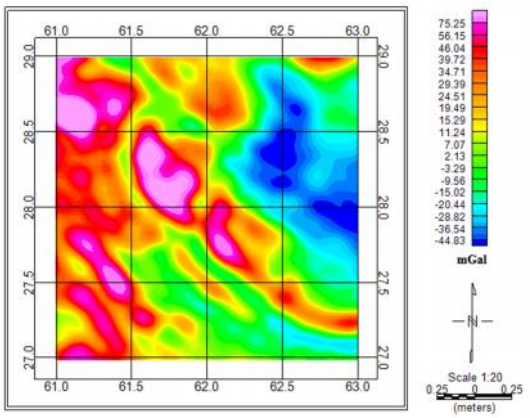

Figure 11. The satelite Bouguer gravity anomaly map of the area under study

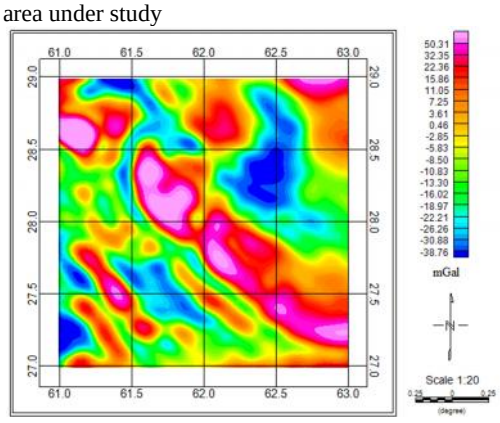

Figure 12. The residual gravity anomalies of the area under study

Results and Discussion

The main purpose of this study is to recognize the most suitable discrete wavelets used in the discrete wavelet decomposition of the gravity data. We have employed the DWT method for approximating edges the source bodies of the gravity anomaly. The analytic results of the gravity data, with and without the random noise, using the DWT at the first level using the Bior1.3, Bior1.5, Bior3.1, Bior3.3, Coif1, Db2, Db3, Dmey, Haar, Sym2 and Sym3 mother wavelets illustrate that the Haar and Bior1.5 mother wavelets perform best in terms of edge detection of the gravity anomaly causative. Accordingly, the GRACE satellite gravity data was decomposed using the DWT based on the Haar and Bior1.5 mother wavelets. The main aim of the analysis of satellite gravity data is revealing the Saravan Fault trend. The maximum values noticeable in the HVC maps superimpose on the linear geological structures of the area under study properly, especially the trend of Saravan Fault. The main conclusions to be drawn from the output is that, firstly, the estimated results of the synthetic and real gravity data decomposition demonstrate the DWT is a useful and powerful for the enhancement of the anomalies border and edge of gravity field. Secondly, the enough resolution of DWT of the satellite gravity data at the first level to delineate the geological features and faults strike is considered. Finally, the point of note is that the satellite gravity data has been proven to be precise enough for regional geological studies. We demonstrate

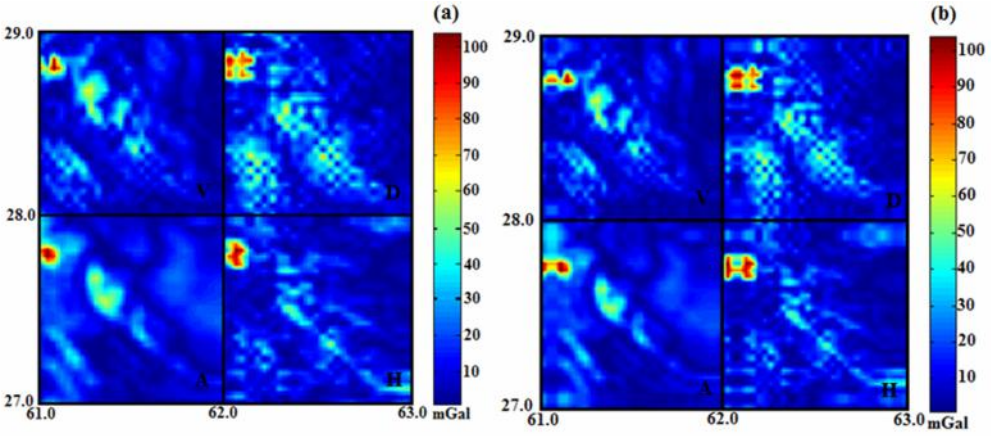

Figure 13. The approximation coefficients (A), horizontal (H), vertical (V) and diagonal (D) components at level 1 from the residual gravity data by the a)Haar and b)Bior 1.5 mother wavelets

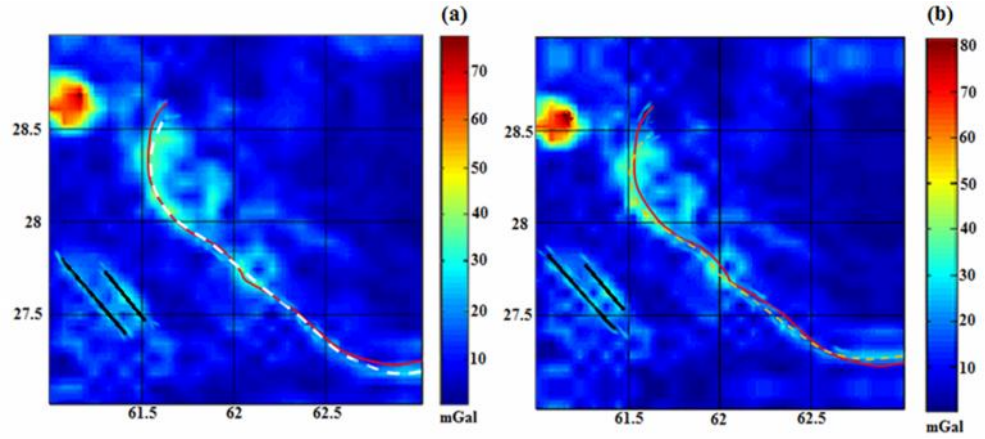

Figure14. HVC of the components of the satellite gravity data DWT by the a)Haar and b)Bior 1.5 wavelets

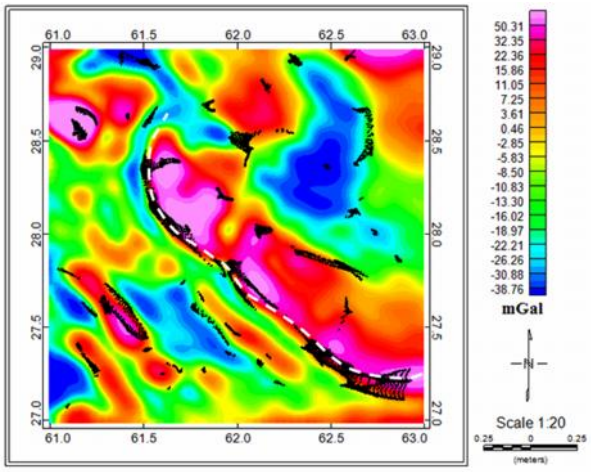

Figure15. The situation of the Euler deconvolution solutions (black points) on the residual gravity map of the area under study. The white dash line indicate the Saravan Fault strike

which using the satellite gravity data can distinguish the faults trend. Thus, the proposed method can also be employed to determine regions where there may be the hidden faults and can be a very good complementary technique for other hidden fault detecting methods.

References

1. Eshaghzadeh, A., Identification of Suitable Discrete Wavelet for Gravity Data Decomposition. *2nd conference of geology and exploration of resources.Shiraz, Iran* (2016).
2. Fedi, M., and Quarta, T., Wavelet analysis for the regionalresidual and local separation of potential field anomalies. *Geophys. Prosp*, **46**: 507–525 (1998).
3. Hornby,P., Boschetti,F., and Horovitz,F.G. Analysis of potential field data in the wavelet domain. *Geophys. J. Internat*, **137**: 175–196 (1999).
4. Leblanc, G.E., and Morris, W.A. Denoising of aeromagnetic data via the wavelet transform. *Geophysics*, **66**: 1793–1804 (2001).
5. Ridsdill-Smith, T. A., and Dentith, M. C. The wavelet transform in aeromagnetic processing. *Geophysics*, **64**: 1003–1013 (1999).
6. Trad,D.O., and Travassos, J. M. Wavelet filtering of magnetotelluric data. *Geophysics*, **65**: 482–491 (2000).
7. Holden, D.J., Archibald, N.J., Boschetti, F., and Jessell, M.W. Inferring geological structures using wavelet-based multiscale edge analysis and forward models. *Explor. Geophys*, **31**: 67–71 (2000).
8. Moreau, F., Gibert, D., Holschneider,M., and Saracco, G. Identification of sources of potential fields with the continuous wavelet transform: basic theory. *J. Geophys. Res*, **104** (B3): 5003–5013 (1999).
9. Deighan, A. J., and Watts, D. R. Ground-roll suppression using the wavelet transform. *Geophysics*, **62**: 1869–1903 (1997).
10. Miller,H.G., and Singh,V. Potential field tilt - a new concept for location of potential field sources. *Journal of Applied Geophysics*, **32**: 213–217 (1994).
11. Wijns, C., Perez, C., and Kowalczyk, P. Theta map: edge detection in magnetic data. *Geophysics*, **70** (4): 39–43 (2005).
12. Verduzco, B., Fairhead, J.D., and Green, C.M. New insights into magnetic derivatives for structural mapping. *The Leading Edge*, **23** (2): 116–119 (2004).
13. Cooper, G.R.J., and Cowan, D.R. Enhancing potential field data using filters based on the local phase. *Computers and Geosciences*, **32**: 1585–1591 (2006).
14. Cooper G.R.J. Balancing images of potential field data. *Geophysics*, **74**: L17–L20 (2009).
15. Ma, G., and Li, L. Edge detection in potential fields with the normalized total horizontal derivative. *Computers & Geosciences*, **41**: 83–87 (2012).
16. Cooper, G.R.J., and Cowan, D.R. Terracing potential field data. *Geophysical Prospecting*, **57**: 1067–1071(2009).
17. Ferreira, F. J. F., J. de Souza, A. B. S. Bongiolo, and L. G. de Castro. Enhancement of the total horizontal gradient of magnetic anomalies using the tilt angle. *Geophysics*, **78**: J33–J41(2013).
18. Cooper, G.R.J., and Cowan, D.R. Edge enhancement of potential-field data using normalized statistics. *Geophysics*,**73**(3): H1–H4 (2008).
19. Lili Li, Guoqing Ma and Xiaojuan Du. Edge Detection in Potential-Field Data by Enhanced Mathematical Morphology Filter. *Pure and Applied Geophysics*, **170** (4): 645-653 (2013).
20. Eshaghzadeh A. Image Edge Detection of the Total Horizontal Gradient of Gravity Data Using the Normalized Tilt Angle. *Geodynamics Research International Bulletin*, **3**(4): P. XXVIII to XXXIII (2015).
21. Eshaghzadeh A. gravity anomalies edge intensification using the tilt angle of the balanced total horizontal derivative. *Geoinformatics: theoretical and applied aspects*, 10-13 May, Kiev, Ukraine, (2016).
22. Pala S.K., and Majumdarb T.J. Geological appraisal over the Singhbhum-Orissa Craton, India using GOCE, EIGEN6-C2 and in-situ gravity data. *International Journal of Applied Earth Observations and Geoinformation*, **35**: 96-119 (2015).
23. Satya N, Soumyashree D.S., Pal S.K., Ujjawal K., Vipin K.P., Majumdar T.J., and Avinash C. Delineation of structural features over a part of the Bay of Bengal using total and balanced horizontal derivative techniques. *Geocarto International*, **32**(1): 1-16 (2016).
24. Mallat, S. Multi frequency Channel decomposition and wavelet models IEEEANS. *Acoustics*, **37**: 209–211 (1989).
25. Addison, P.S.: The Illustrated Wavelet Handbook: Introductory Theory and Applications in Science, Engineering, Medicine and Finance. Institute of Physics Publishing, Bristol, UK. (2002)
26. Alp, H., Albora, A.M., and Tur, H. A view of tectonic structure and gravity anomalies of Hatay region southern Turkey using wavelet analysis. *J. Appl. Geophys*, **75**: 498–505 (2011).
27. Daubechies, I. Ten Lectures on Wavelets. *Vol. 61 of CBMS-NSF Regional Conference Series in Applied Mathematics*, SIAM Publications, Philadelphia, (1992).
28. Farimani, F.A.A., Dehghan, S., Role of Saravan Thrust Fault on Formation and Development of Saravan Catchment Basin. *Geography And Development.* **12** (35): 19-31 (2014).